

# Effect of boundary scattering on the thermal conductivity of TiNiSn-based half-Heusler alloys

S. Bhattacharya,\* M. J. Skove, M. Russell, and T. M. Tritt  
*Department of Physics, Clemson University, Clemson, South Carolina 29634, USA*

Y. Xia, V. Ponnambalam, and S. J. Poon  
*Department of Physics, University of Virginia, Charlottesville, Virginia 22901, USA*

N. Thadhani  
*Materials Science and Engineering, Georgia Institute of Technology, Atlanta, Georgia 30332, USA*

(Received 22 December 2007; published 30 May 2008)

TiNiSn-based half-Heusler alloys have been of significant interest for their potential as thermoelectric materials. They exhibit promising electronic transport properties as revealed through high Seebeck coefficient and moderate electrical resistivity values. The chief disadvantage of these materials is a comparatively high lattice thermal conductivity. Attempts to “tune” the lattice thermal conductivity ( $\kappa_L$ ) in these materials have led to the comparison and analysis of the thermal conductivity of two series of Ti- and Zr-based half-Heusler alloys. In the first series,  $\text{Ti}_{1-y}\text{Zr}_y\text{NiSn}_{0.95}\text{Sb}_{0.05}$ , a significant reduction in  $\kappa_L$  is observed, with the substitution of large concentrations of Zr ( $y \geq 25\%$ ) at Ti site, which is most likely due to mass fluctuation scattering. In the second series,  $\text{TiNiSn}_{1-x}\text{Sb}_x$ , a nonsystematic increase in  $\kappa_L$  is observed, with minute amounts of Sb doping ( $x \leq 5\%$ ) at the Sn site. Extensive microstructural analysis in a  $\text{TiNiSn}_{1-x}\text{Sb}_x$  series reveals a correlation between  $\kappa_L$  and the average grain diameter in these materials, which is in good agreement with theoretical predictions related to phonon boundary scattering. In addition, a comparison of the calculated phonon mean free path in each of the series of compounds shows some insight into the two different phonon scattering mechanisms.

DOI: [10.1103/PhysRevB.77.184203](https://doi.org/10.1103/PhysRevB.77.184203)

PACS number(s): 65.40.-b, 63.20.kp, 61.72.Mm

## I. INTRODUCTION

The half-Heusler alloys are a group of ternary intermetallic compounds with the general formula  $MM'X$ , which is composed of transition metals ( $M = \text{Zr, Hf, Ti, V, Nb, Mn}$  and  $M' = \text{Fe, Co, Ni}$ ) and a nonmetal or a nonmagnetic metal ( $X = \text{Sn, Sb, In, Ge, Al}$ ).<sup>1</sup> The half-Heusler alloys exhibit the cubic  $\text{MgAgAs}$  ( $C1_b$ ) type of crystal structure consisting of 3 filled and 1 vacant interpenetrating fcc sublattices with 12 atoms in a unit cell. The third fcc structure is shifted by one-fourth of the unit cell from the body diagonal of the rocksalt structure.<sup>2</sup> The half-Heusler alloys are structurally comparable to their parent compounds, the Heusler alloys ( $MM'_2X$ ), which have two sublattices occupied by  $M'$  atoms, and thus there is no vacant sublattice. A half-Heusler alloy differs from the metallic Heusler alloy in being semiconducting or semimetallic due to the presence of a “hybridization gap” at the Fermi level.<sup>3</sup> The half-Heusler alloys exhibit unusual electronic, optical, and magnetic transport properties.<sup>4-6</sup>

The MNiSn ( $M = \text{Ti, Zr, Hf}$ ) half-Heusler alloys have been of significant interest for their potential as thermoelectric (TE) materials for several years.<sup>7-9</sup> The combination of high thermopower ( $\alpha \approx -60$  to  $-150 \mu\text{V/K}$ ) and low electrical resistivity ( $\rho = 1/\sigma \approx 1-0.1 \text{ m}\Omega \text{ cm}$ ) in the TiNiSn-based half-Heusler alloys has resulted in promising TE power factor ( $\alpha^2\sigma T$ ) of about  $0.7-1.0 \text{ W m}^{-1} \text{ K}^{-1}$  at 300 K. Optimized doping of 5% Sb at Sn site has resulted in the largest power factors ( $\alpha^2\sigma T \approx 1.0 \text{ W m}^{-1} \text{ K}^{-1}$  at 300 K and  $\approx 4.5 \text{ W m}^{-1} \text{ K}^{-1}$  at 650 K in the  $\text{TiNiSn}_{0.95}\text{Sb}_{0.05}$ .<sup>10</sup> Other groups have also reported promising thermoelectric properties in the half-Heusler alloys. A TE figure of merit or ZT

( $=\alpha^2\sigma T/\kappa$ )  $\approx 0.7$  at 800 K has been reported in the  $\text{Zr}_{0.5}\text{Hf}_{0.5}\text{Ni}_{0.8}\text{Pd}_{0.2}\text{Sn}_{0.99}\text{Sb}_{0.01}$  by Shen *et al.*<sup>11</sup> The highest value of  $\text{ZT} = 0.81$  at  $T = 1025 \text{ K}$  was observed by Culp *et al.*<sup>12</sup> in the half-Heusler alloys for a composition of  $\text{Hf}_{0.75}\text{Zr}_{0.25}\text{NiSn}_{0.975}\text{Sb}_{0.025}$ , which was found to exceed the goal set for industrial purposes by the SiGe alloys.

The TiNiSn half-Heusler alloys exhibit a lattice parameter of  $5.94 \text{ \AA}$ .<sup>13</sup> The result of an “unfilled” structure in the half-Heusler alloys due to the vacant Ni sublattice leads to interesting band-structure properties. A narrow energy band gap ( $0.1-0.2 \text{ eV}$ ) (Refs. 5 and 7) at the Fermi level, possibly due to an overlap between the  $d$ ,  $d$  [ $\text{Ti}(3d^24s^2)$ ,  $(\text{Ni}(3d^84s^2))$ ], and  $p$  and  $d$  [ $\text{Ti}(3d^24s^2)$  or  $\text{Ni}(3d^84s^2)$  and  $\text{Sn}(5s^25p^2)$ ] wave functions leads to novel electronic transport properties.<sup>2</sup> The position of the Fermi level with respect to the gap determines whether these compounds are semiconducting or metallic. A small band gap near the Fermi level not only makes the band structure sensitive to various chemical substitutions but also accounts for the “tunability” and variability of the electrical resistivity ( $\rho \approx 1/\sigma \approx 0.1-8 \text{ m}\Omega \text{ cm}$ ) at room temperature.<sup>10</sup>

Although the electrical transport properties in the Ti-based half-Heusler alloys reveal positive results, the lattice thermal conductivity observed ( $\kappa_L \approx 10 \text{ W m}^{-1} \text{ K}^{-1}$  at 300 K) is quite high and needs to be further reduced.<sup>14</sup> An ideal thermoelectric material requires a high Seebeck coefficient ( $\alpha \approx 100-300 \mu\text{V K}^{-1}$ ) and favorable electrical conductivity ( $\sigma \approx 10^2-10^4 \Omega \text{ cm}^{-1}$ ) as exhibited by semimetals or semiconductors with an optimal energy gap ( $E_g \approx 0.25 \text{ eV}$ ).<sup>15</sup> The Seebeck coefficient, from Mott’s equation for metals, is given by  $\alpha = (\pi^2/3)(k^2T/e)[d(\ln \sigma)/dE]_{E=E_F}$ , where  $\sigma$  is the electrical conductivity and  $\alpha$  is proportional to

the logarithmic derivative of the electrical conductivity at the Fermi energy.<sup>16</sup> By using a simple theory for nearly free electrons and assuming charge-carrier scattering distance to be independent of energy,<sup>17,18</sup> the Seebeck coefficient may be expressed as  $\alpha = (8\pi^2 k_B^2 / 3eh^2) m^* T (\pi/3n)^{2/3}$ , where  $k_B$  is the Boltzmann constant,  $m^*$  is the effective mass, and  $n$  is the carrier concentration. For good conductors,  $n$  is considerably large and also the electrical conductivity ( $\sigma = ne\mu$ ), which is thus inversely related to the Seebeck coefficient. However, optimizing these two parameters via “doping” or chemical substitution proves to be an effective option. To further maximize ZT, several methods of “tuning” the lattice thermal conductivity by increasing phonon scattering via mass fluctuation or grain boundary scattering are investigated.<sup>19,20</sup>

## II. EXPERIMENTAL PROCEDURE

Alloys of different compositions were prepared by arc melting appropriate quantities of elements together. Titanium (4N purity), zirconium (3N purity), antimony (5N purity), tin (5N purity), and nickel (5N purity) metal powders were mixed together and pressed into a pellet. This pellet was arc melted on a water-cooled copper hearth under argon atmosphere. The resulting button was remelted two or three times after turning the pellet to ensure homogeneity. The button was wrapped in a Ta foil and sealed in an evacuated quartz tube for annealing. For a “standard” alloy, a short term annealing at 900 °C for 14 h and a long term annealing at 750 °C for one week were carried out. High quality single-phase polycrystalline samples were confirmed by x-ray diffraction. Ball milling was carried out under argon pressure for 10 h by using a Spex mixer mill (model 8000). The milled powders were shock consolidated using a three-capsule plate-impact compaction fixture, with an 80 mm diameter single stage gas gun. Prior to consolidation, the powders were pressed in the capsules to about 60%–63% of their theoretical maximum density and capped with the plugs. Compaction was performed at a measured velocity of 508 m/s ( $\sim 5$ – $7$  GPa calculated pressure), which yields 10 mm diameter by 3-mm-thick fully dense compacts. Figure 1 shows the x-ray diffraction pattern for a standard and ball-milled and shock-compacted (BM-SC) TiNiSn<sub>0.95</sub>Sb<sub>0.05</sub> half-Heusler alloy. A small rectangular piece ( $2 \times 2 \times 8$  mm<sup>3</sup>) was cut from each ingot of different compositions to measure resistivity, thermopower, and thermal conductivity.

Resistivity and thermopower are simultaneously measured in a closed cycle helium cryostat from 10 to 300 K, and the specific technique is described in detail elsewhere.<sup>21</sup> The thermal conductivity is also measured from 10 to 300 K using a separate custom designed system by using a steady state technique. The mounting and measurement technique and instrumentation are also described in detail elsewhere.<sup>22</sup>

## III. EXPERIMENTAL RESULTS AND DISCUSSIONS

An optimal doping of 5% Sb in TiNiSn<sub>0.95</sub>Sb<sub>0.05</sub> exhibits the highest power factor ( $\alpha^2 \sigma T \approx 4.5$  W m<sup>-1</sup> K<sup>-1</sup> at 650 K) in this series of half-Heusler alloys. However, a com-

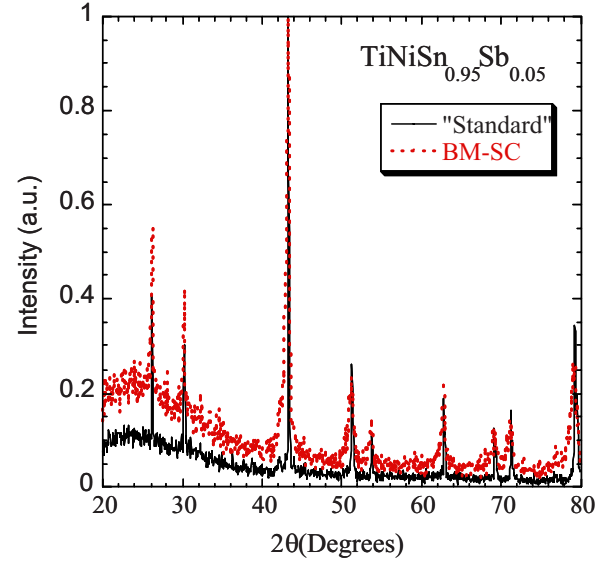


FIG. 1. (Color online) X-ray diffraction pattern for a standard and ball-milled and shock compacted (BM-SC) TiNiSn<sub>0.95</sub>Sb<sub>0.05</sub> half-Heusler alloy.

paratively high lattice thermal conductivity<sup>14</sup> ( $\kappa_L$ )  $\approx 10$  W m<sup>-1</sup> K<sup>-1</sup> (almost a factor of 5 higher than most good TE materials)<sup>23</sup> is a drawback that has been difficult to overcome in these materials. The thermal conductivity in the half-Heusler alloys chiefly consists of the lattice contribution ( $\kappa_L \approx 90\%$  of the total  $\kappa_T$ ), which is indirectly calculated using the Wiedemann Franz relation ( $\kappa_E = L_O \sigma T$ , where  $L_O = 2.45 \times 10^{-8}$  V<sup>2</sup>/K<sup>2</sup> is the Lorentz number and  $\kappa_L = \kappa_T - \kappa_E$ ).

The effect of substituting large concentrations of Zr ( $\geq 20\%$ ) at the Ti site on lattice thermal conductivity in Ti<sub>1-y</sub>Zr<sub>y</sub>NiSn<sub>0.95</sub>Sb<sub>0.05</sub> series is studied, keeping the optimal Sb doping (5%) a constant. The key to a large TE figure of merit is not only to reduce the high  $\kappa_L$  but also to maintain the overall promising electronic transport properties observed through high power factors ( $\alpha^2 \sigma T$ ). Figure 2(a) shows  $\kappa_L$  as a function of temperature for the series Ti<sub>1-y</sub>Zr<sub>y</sub>NiSn<sub>0.95</sub>Sb<sub>0.05</sub> ( $y=0.0, 0.25, 0.5, 0.6, 0.75, \text{ and } 1.0$ ). The end elements of the series, TiNiSn<sub>0.95</sub>Sb<sub>0.05</sub> and ZrNiSn<sub>0.95</sub>Sb<sub>0.05</sub>, exhibit the highest  $\kappa_L$  values as expected. The temperature dependence as well as the magnitude ( $\kappa_T \approx 16$  W m<sup>-1</sup> K<sup>-1</sup> at 300 K) of the total thermal conductivity in ZrNiSn<sub>0.95</sub>Sb<sub>0.05</sub> ( $y=1.0$ ) are in excellent agreement with the measurement of thermal conductivity of a week long annealed ZrNiSn reported by Uher *et al.*<sup>8</sup> The minimal amount of Sb doping (5%) in ZrNiSn<sub>0.95</sub>Sb<sub>0.05</sub> has very little effect on  $\kappa_L$  compared to that of ZrNiSn. In the intermediate alloyed compounds Ti<sub>1-y</sub>Zr<sub>y</sub>NiSn<sub>0.95</sub>Sb<sub>0.05</sub> ( $y=0.25, 0.5, 0.6, \text{ and } 0.75$ ), the lattice thermal conductivity is highly reduced (almost by 50%), most likely due to the difference in the atomic masses of Zr ( $M_{Zr}=91$  g/mol) and Ti ( $M_{Ti}=48$  g/mol). The difference in the atomic radii of Zr (2.16 Å) and Ti (2 Å) may also affect  $\kappa_L$  due to strain field scattering effects, but this effect has not been investigated any further. Figure 2(b) shows the lattice thermal conductivity ( $\kappa_L$ ) at room temperature in the Ti<sub>1-y</sub>Zr<sub>y</sub>NiSn<sub>0.95</sub>Sb<sub>0.05</sub> as a function of the nominal Zr concentrations ( $y$ ). The overall

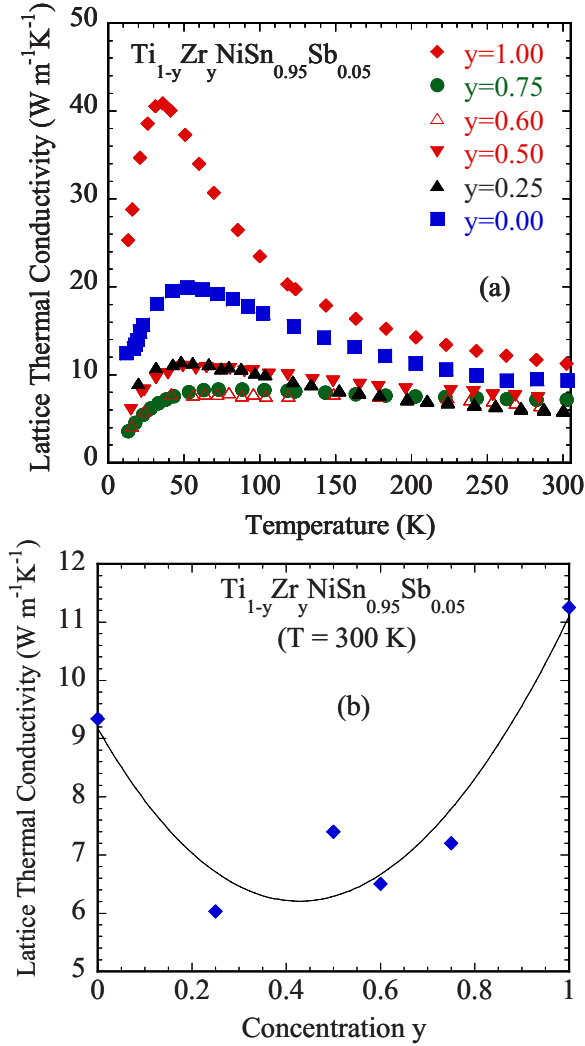


FIG. 2. (Color online) Lattice thermal conductivity vs (a) temperature (b) nominal concentration of Zr substitution in the  $\text{Ti}_{1-y}\text{Zr}_y\text{NiSn}_{0.95}\text{Sb}_{0.05}$  series.

effect of Zr substitution is to disorder the crystal lattice, as evident from a large, systematic reduction in  $\kappa_L$ , with a maximal mass disorder near a concentration of 50% Zr at Ti site, pointing toward mass fluctuation scattering. The electronic transport properties in the  $\text{Ti}_{1-y}\text{Zr}_y\text{NiSn}_{0.95}\text{Sb}_{0.05}$  series reveal that the parent compositions ( $\text{TiNiSn}_{0.95}\text{Sb}_{0.05}$  and  $\text{ZrNiSn}_{0.95}\text{Sb}_{0.05}$ ) exhibit the upper limits of the power factors ( $\alpha^2\sigma T$ ), decreasing in magnitude with increasing Zr substitution at the Ti site.<sup>14</sup> The Seebeck coefficients in this series are negative, ranging from  $-45$  to  $-70$   $\mu\text{V}/\text{K}$  with the highest thermopower being for  $\text{TiNiSn}_{0.95}\text{Sb}_{0.05}$ .<sup>10</sup> The resistivity ( $\rho=1/\sigma$ ) exhibits a semimetallic nature, increasing with increase in temperature. Resistivity values lie between 0.15 and 0.2  $\text{m}\Omega\text{ cm}$  at room temperature with the highest value for  $y=0.75$ .  $\text{TiNiSn}_{0.95}\text{Sb}_{0.05}$  remains the optimal composition in this series of samples with the highest power factor ( $\approx 1.0$   $\text{W m}^{-1}\text{K}^{-1}$  at  $T=300$  K).<sup>14</sup>

Figure 3(a) shows  $\kappa_L$  vs temperature in the  $\text{TiNiSn}_{1-x}\text{Sb}_x$  series with minute ( $x \leq 5\%$ ) amounts of Sb doping at Sn site. For these low concentrations of Sb doping in the  $\text{TiNiSn}_{1-x}\text{Sb}_x$  ( $x=0.0, 0.005, 0.02, 0.03, \text{ and } 0.05$ ), the room

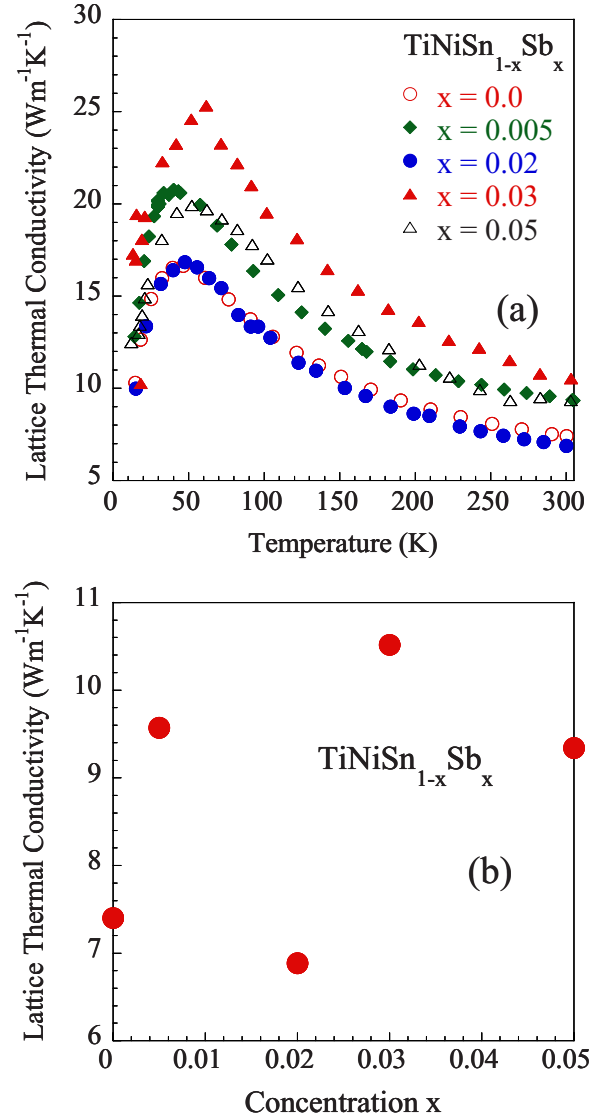


FIG. 3. (Color online) Lattice thermal conductivity as a function of (a) temperature and (b) concentration of Sb doping in the  $\text{TiNiSn}_{1-x}\text{Sb}_x$  series.

temperature values of thermal conductivity vary nonsystematically over a range from approximately  $6$ – $15$   $\text{W m}^{-1}\text{K}^{-1}$ . Pure  $\text{TiNiSn}$  exhibits a thermal conductivity of about  $8$   $\text{W m}^{-1}\text{K}^{-1}$  at room temperature, in good agreement with the thermal conductivity of  $\text{TiNiSn}$  measured by other groups ( $9$   $\text{W m}^{-1}\text{K}^{-1}$  at  $300$  K).<sup>9</sup> Figure 3(b) shows  $\kappa_L$  as a function of concentration ( $x$ ) of Sb doping. These results in Figs. 3(a) and 3(b) seem inconclusive at first, as is expected that  $\kappa_L$  in this series would be of similar magnitudes at all temperatures due to the close proximity of Sb ( $M_{\text{Sb}}=121.8$  g/mol) and Sn ( $M_{\text{Sn}}=118.7$  g/mol) in the Periodic Table.

#### IV. MICROSTRUCTURAL ANALYSIS

An extensive investigation of microstructure in  $\text{TiNiSn}_{1-x}\text{Sb}_x$  series by Bhattacharya *et al.*<sup>19</sup> has established a direct correlation of  $\kappa_L$  with the average grain diameter ( $D$ )

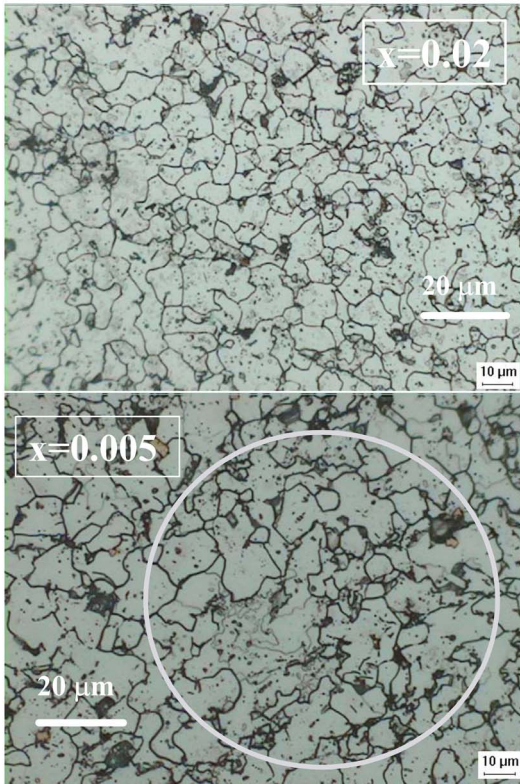
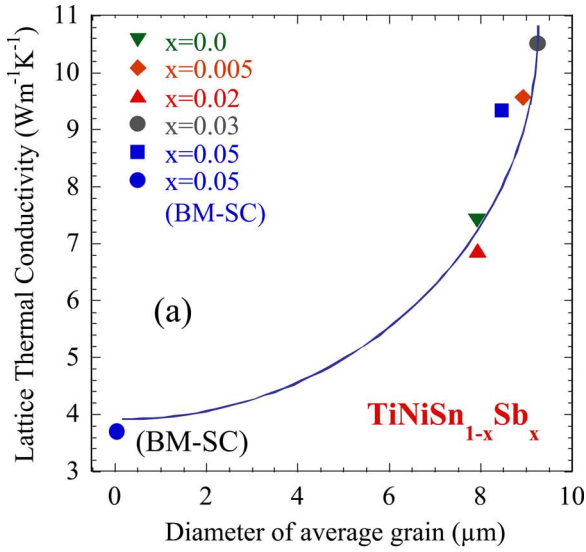


FIG. 4. (Color online) (a) Lattice thermal conductivity as a function of the average grain diameter in the  $\text{TiNiSn}_{1-x}\text{Sb}_x$  series. (b) Characteristic grain structures in  $\text{TiNiSn}_{1-x}\text{Sb}_x$  ( $x=0.02$  and  $0.005$ ). The average grain sizes calculated using standard ASTM techniques (Ref. 30).

in these materials. In Fig. 4(a), for the standard  $\text{TiNiSn}_{1-x}\text{Sb}_x$  compounds,  $\kappa_L$  systematically decreases with a decrease in grain diameter ( $D \leq 10 \mu\text{m}$ ) even with the small variation of grain size. This plot also includes a BM-SC  $\text{TiNiSn}_{0.95}\text{Sb}_{0.05}$  sample, with  $D \leq 0.05 \mu\text{m}$  and a remarkably low  $\kappa_L$  for a half-Heusler alloy ( $\kappa_L \leq 4 \text{ W m}^{-1} \text{ K}^{-1}$ ). The line is a guide for the eyes showing the systematic variation of  $\kappa_L$  with  $D$ . Figure 4(b) exhibits characteristic grain structures for  $\text{TiNiSn}_{1-x}\text{Sb}_x$  ( $x=0.02$  and  $0.005$ ). Figure 5(a) shows the

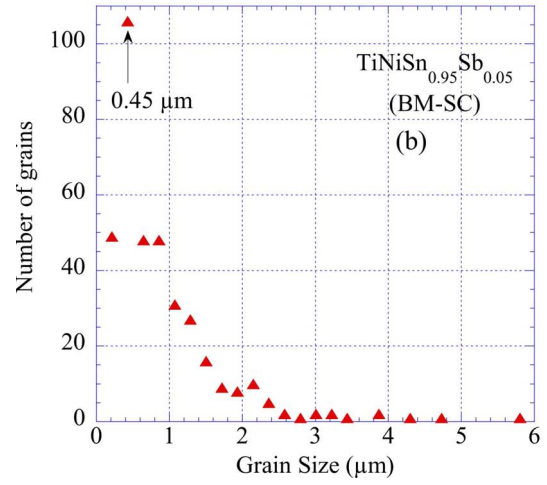
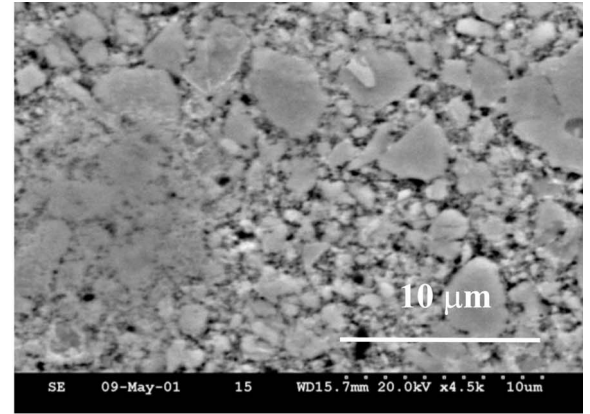


FIG. 5. (Color online) (a) SEM images of BM-SC  $\text{TiNiSn}_{0.95}\text{Sb}_{0.05}$ . (b) BM-SC samples yield very small grain sizes ( $D < 1 \mu\text{m}$ ).

scanning electron microscopy (SEM) images of the BM-SC  $\text{TiNiSn}_{0.95}\text{Sb}_{0.05}$ . The plot of number of grains as a function of grain size in Fig. 5(b) shows an average grain size  $D < 1 \mu\text{m}$ . The correlation of  $\kappa_L$  with the average grain diameter in the Ti-based half-Heusler alloys is in good agreement with the theoretical predictions of Goldsmid and co-workers,<sup>24,25</sup> which are related to phonon boundary scattering of half-Heusler alloys, where  $\kappa_L$  is predicted to be sensitive to the grain size ( $D \leq 10 \mu\text{m}$ ) of the material. The electrical resistivity in the  $\text{TiNiSn}_{1-x}\text{Sb}_x$  series is found to vary with the concentration of Sb doping, decreasing uniformly with increase in Sb substituted at the Sn site.<sup>10</sup>

The grain structures of the  $\text{Ti}_{1-y}\text{Zr}_y\text{NiSn}_{0.95}\text{Sb}_{0.05}$  series have been further examined to compare to that of the  $\text{TiNiSn}_{1-x}\text{Sb}_x$  series to understand the effects of different phonon scattering mechanisms on  $\kappa_L$  in the Zr-substituted compounds. The  $\text{Ti}_{1-y}\text{Zr}_y\text{NiSn}_{0.95}\text{Sb}_{0.05}$  compounds were polished and etched with a suitable grain boundary etchant for about 25 s and observed under the SEM. Figure 6(a) shows the SEM image of grain structure of  $\text{Ti}_{1-y}\text{Zr}_y\text{NiSn}_{0.95}\text{Sb}_{0.05}$  ( $y=0.25$ ). From our microstructural analysis, the  $\text{Ti}_{1-y}\text{Zr}_y\text{NiSn}_{0.95}\text{Sb}_{0.05}$  series exhibits a much larger average grain size ( $D \geq 50 \mu\text{m}$ ) as compared to the  $\text{TiNiSn}_{1-x}\text{Sb}_x$  compounds ( $D \leq 10 \mu\text{m}$ ) [Fig. 4(b)]. The grains in the Zr-substituted compounds are observed to have

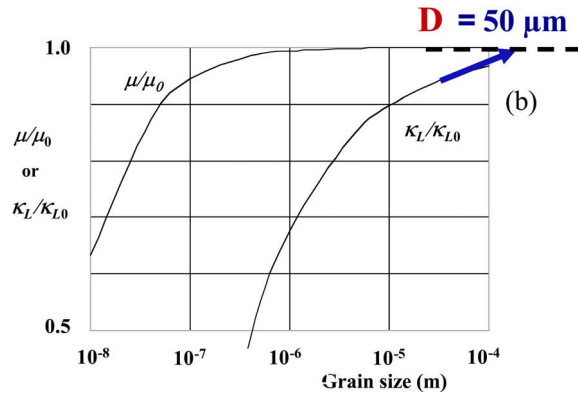
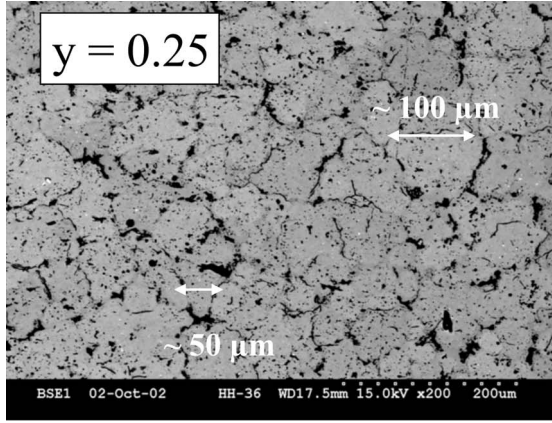


FIG. 6. (Color online) Average grain diameter ( $D > 50 \mu\text{m}$ ) in  $\text{Ti}_{1-y}\text{Zr}_y\text{NiSn}_{0.95}\text{Sb}_{0.05}$  compounds (a)  $y=0.25$ . (b) The theoretical predictions of Goldsmid *et al.* (Ref. 25) suggest that  $k_L$  decreases much faster than the mobility below a grain size of about  $10 \mu\text{m}$ . Our experimental results show that the grain size in the  $\text{Ti}_{1-y}\text{Zr}_y\text{NiSn}_{0.95}\text{Sb}_{0.05}$  series is ( $D \geq 50 \mu\text{m}$ ), where boundary scattering is not predicted to be a prominent phonon scattering mechanism.

distinct light and dark regions possibly due to inhomogeneous Zr rich regions (microprobe analysis).

From the theoretical predictions of Goldsmid *et al.*<sup>24</sup> as observed in Fig. 6(b),  $k_L$  decreases with a decrease in grain diameter at slightly higher values than does the carrier mobility. The dependence of  $k_L$  is most prominent for a grain size ( $D \leq 10 \mu\text{m}$ ) but is almost independent of size at larger grain diameters ( $D \geq 50 \mu\text{m}$ ). Our experimental observations of the microstructure and the thermal conductivity measurements in the  $\text{TiNiSn}_{1-x}\text{Sb}_x$  also show a dependence on grain size ( $D \leq 10 \mu\text{m}$ ). For  $\text{Ti}_{1-y}\text{Zr}_y\text{NiSn}_{0.95}\text{Sb}_{0.05}$  series, where the average grain size is  $D \geq 50 \mu\text{m}$ ,  $k_L$  is more sensitive to mass fluctuation scattering, and boundary scattering is not a prominent phonon scattering mechanism in this case. These results are in very good agreement with the theoretical predictions on boundary scattering of phonons in the half-Heusler alloys by Goldsmid and co-workers.<sup>24,25</sup>

## V. DISCUSSIONS OF THERMAL CONDUCTIVITY

The temperature dependence of lattice thermal conductivity in a perfect crystal exhibits a well-defined peak at low

temperatures. The different scattering mechanisms that mold the temperature dependence of the lattice thermal conductivity  $\kappa_L(x)$  are given in Eqs. (1)–(3), where  $x = \hbar\omega/k_B T$  or the reduced phonon frequency,<sup>26,27</sup>

$$\kappa_L(x) = \frac{k_B}{2\pi^2 v_s} \left( \frac{k_B T}{\hbar} \right) \int_0^{\Theta_D/T} \frac{x^4 e^x}{\tau_{ph}^{-1} (e^x - 1)^2} dx, \quad (1)$$

$$\tau_{ph}^{-1} = \tau_{MF}^{-1} + \tau_U^{-1} + \tau_B^{-1}, \quad (2)$$

$$\tau_{ph}^{-1} = A\omega^4 + B e^{-\Theta_D/T} T^3 \omega^2 + v_s/D. \quad (3)$$

In the above equations,  $A$  and  $B$  are constants,  $\omega$  is the phonon angular frequency,  $\tau_{MF}$  ( $\approx \omega^{-4}$ ) represents the relaxation time due to mass fluctuation scattering via impurities or point defects,  $\tau_U$  is the relaxation time due to umklapp scattering, and  $\tau_B$  ( $\approx v_s/D$ ) is the relaxation time due to phonon boundary scattering. It must be noted that the phonon relaxation time due to boundary scattering ( $\tau_B \approx v_s/D$ ) is independent of the phonon frequency, unlike the other two phonon scattering mechanisms.

At lower temperatures ( $T \ll \Theta_D$ ), the average phonon frequency is low and long wavelength phonons are present, which are mostly unaffected by both point defects and other phonon interactions. These long wavelength phonons at lower temperatures are chiefly scattered by grain boundaries (polycrystalline) and crystal dimensions (single crystals). With a change in temperature, the phonon spectrum also changes. The short wavelength phonons are present at higher temperatures where the maximum frequency possible is  $\omega_{\text{max}}$  (Debye frequency). The scattering of phonons mostly depends on the size (or difference in mass) of the irregularity in the crystal lattice. When a point defect is larger than the phonon wavelength, mass fluctuation scattering, comparable to Rayleigh scattering,<sup>28</sup> occurs, which reduces the thermal conductivity of the material.

## VI. MEAN FREE PATH CALCULATIONS

In order to completely understand the two different phonon scattering mechanisms and their effects on the lattice thermal conductivity ( $\kappa_L$ ), a theoretical estimation of the mean free paths in the two series of half-Heusler alloys,  $\text{TiNiSn}_{1-x}\text{Sb}_x$  and  $\text{Ti}_{1-y}\text{Zr}_y\text{NiSn}_{0.95}\text{Sb}_{0.05}$ , is presented by using the classical kinetic theory relation,

$$\kappa_L = \frac{1}{3} c_v v_s \ell_{ph}. \quad (4)$$

The mean free path ( $\ell_{ph}$ ) of phonons is estimated using the measured values of the specific heat capacity per unit volume of phonons ( $c_v$ ), the lattice thermal conductivity ( $\kappa_L$ ), and the calculated values of the phonon velocity ( $v_s$ ) (or the velocity of sound through a material). The velocity of sound is theoretically calculated using the relation<sup>24</sup>

$$v = \frac{2k_B a \Theta_D}{h}, \quad (5)$$

where,  $k_B$  is the Boltzmann constant,  $a$  the lattice constant, and  $\Theta_D$  is the Debye temperature. The velocity of sound [Eq.

(5)] arises from the relation ( $k_B\Theta_D = \hbar\omega$ ) with the assumption that the phonon wavelength  $\lambda = 2a$ . The mean free paths at different temperatures are calculated using the measured values of  $\kappa_L$  and the measured specific heat capacity value. The electronic component of the molar specific heat capacity ( $\gamma T$ ) is subtracted from the measured total specific heat capacity to get the lattice component ( $C_{ph}$ ), which is used in our calculations.

Some approximations in the calculations of both the velocity of sound and the phonon mean free path in these materials are discussed below. The molar heat capacity at constant pressure ( $C_p$ ) is measured under a high vacuum ( $<1$  mTorr) and it is assumed that  $C_p \approx C_v$  for a solid sample. The lattice constant ( $a = 5.93$  Å) is used for the  $\text{TiNiSn}_{1-x}\text{Sb}_x$  compounds.<sup>9</sup> The densities used for unit conversion of the molar specific heat capacity (J/mol K) to specific heat capacity (J/m<sup>3</sup> K) for standard  $\text{TiNiSn}_{1-x}\text{Sb}_x$  compounds are 7.1 g/cm<sup>3</sup> and for the BM-SC ( $\text{TiNiSn}_{0.95}\text{Sb}_{0.05}$ )  $\approx 6.5$  g/cm<sup>3</sup>. The density of  $\text{ZrNiSn}_{0.95}\text{Sb}_{0.05}$  calculated using lattice constant  $a = 6.11$  Å is 7.8 g/cm<sup>3</sup>. A linear interpolation between the densities of  $\text{TiNiSn}_{0.95}\text{Sb}_{0.05}$  and  $\text{ZrNiSn}_{0.95}\text{Sb}_{0.05}$  is obtained to estimate the densities of the  $\text{Ti}_{1-y}\text{Zr}_y\text{NiSn}_{0.95}\text{Sb}_{0.05}$  series. The thermal conductivity data are measured to about 10 K in a cryocooler system. The low temperature data used for our calculations have been linearly extrapolated to 4 K. The low temperature data in  $\text{TiNiSn}_{1-x}\text{Sb}_x$  ( $x = 0.03$ ) is somewhat noisy and hence a reliable extrapolation is not possible.

From our calculations, it is observed [Fig. 7(a)] that the values of the mean free path in the  $\text{TiNiSn}_{1-x}\text{Sb}_x$  series are comparable to the grain diameters (obtained from previous microstructural analysis)<sup>19</sup> when we linearly extrapolate the  $\kappa_L$  data to  $T \approx 4$  K. Within the limits of the uncertainties in the extrapolation of the thermal conductivity data to these low temperatures as shown by the error bars, this calculation certainly emphasizes the correlation of  $\kappa_L$  with the average grain diameters (as observed through microstructural analysis) and not with the concentration of Sb doping. Phonon boundary scattering is thus a more prominent scattering phenomenon in the  $\text{TiNiSn}_{1-x}\text{Sb}_x$  series, especially at low temperatures when all the other scattering phenomena are a minimum.

In contrast, in the  $\text{Ti}_{1-y}\text{Zr}_y\text{NiSn}_{0.95}\text{Sb}_{0.05}$  ( $y = 0.25, 0.5, 0.6,$  and  $0.75$ ) series, the alloyed compounds exhibit a mean free path of as low as  $3.0$   $\mu\text{m}$  ( $y = 0.6$ ) even though they exhibit a much larger grain diameter ( $D > 50$   $\mu\text{m}$ ). Obviously, phonon boundary scattering is not prominent in this case. In  $\text{ZrNiSn}_{0.95}\text{Sb}_{0.05}$ , where there should be no mass fluctuation scattering affecting thermal conduction (with negligible effects of any isotopic fluctuations), the mean free path is calculated to be about  $26$   $\mu\text{m}$  at  $T \approx 4$  K and a grain size  $D \geq 50$   $\mu\text{m}$  is observed. From our experimental observations, mass fluctuation scattering is understood to be a more prominent scattering mechanism in the Zr-substituted series due to a larger difference in atomic masses of Zr ( $M_{\text{Zr}} = 91$  g/mol) and Ti ( $M_{\text{Ti}} = 48$  g/mol). In order to find a correlation between the mean free paths and the concentrations of Zr substitution, we write the total relaxation time ( $1/\tau_{ph}$ ) for the series of  $\text{Ti}_{1-y}\text{Zr}_y\text{NiSn}_{0.95}\text{Sb}_{0.05}$  to be equal to the sum of the inverse relaxation times limited by the three

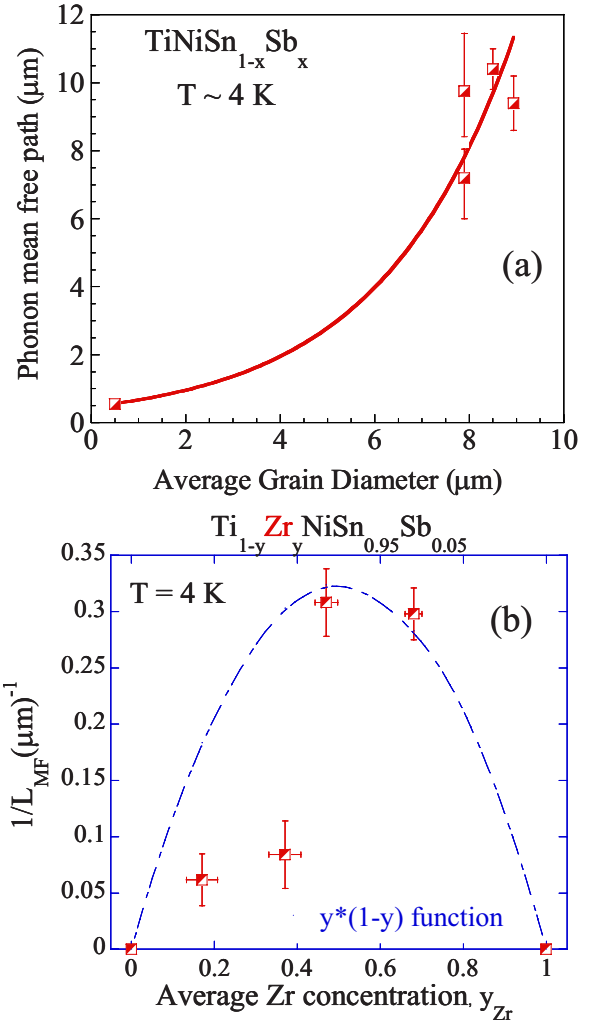


FIG. 7. (Color online) (a) Correlation between calculated mean free path and average grain diameter obtained from microstructural analysis (b)  $1/L_{MF}$ , ( $L_{MF}$  is the calculated phonon mean free path limited by mass fluctuation scattering) vs concentration ( $y$ ) of Zr substitution. The dotted lines represent a  $y^*(1-y)$  function. The error bars represent uncertainty in the extrapolation of  $\kappa_L$  at low temperatures.

phonon scattering mechanisms indicated by  $U$  (umklapp),  $B$  (boundary), and  $MF$  (mass fluctuation),

$$\frac{1}{\tau_{ph}} = \frac{1}{\tau_U} + \frac{1}{\tau_B} + \frac{1}{\tau_{MF}}. \quad (6)$$

In the parent compound  $\text{TiNiSn}_{0.95}\text{Sb}_{0.05}$ , ( $y = 1$ ) where there is no additional mass fluctuation scattering arising from any Zr atoms (considering very little mass fluctuation scattering arising from the minute amount of Sb doping), we may assume the relaxation time ( $1/\tau'_{ph}$ ) to be

$$\frac{1}{\tau'_{ph}} = \frac{1}{\tau_U} + \frac{1}{\tau_B}. \quad (7)$$

Subtracting Eq. (7) from Eq. (6), we obtain the contribution to the relaxation time limited by mass fluctuation scattering alone, arising from large amounts of Zr substitution at Ti site,

$$\frac{1}{\tau_{MF}} = \frac{1}{\tau_{ph}} - \frac{1}{\tau'_{ph}}. \quad (8)$$

The contribution to mean free path ( $L_{MF}$ ) limited by mass fluctuation scattering is calculated below, where the mean free path ( $L$ ) is proportional to the relaxation time ( $\tau$ ),

$$\frac{1}{L_{MF}} = \frac{1}{L_{doped}} - \frac{1}{L_{pure}}, \quad (9)$$

where  $L_{doped}$  refers to the calculated mean free paths of the Zr-substituted compounds in  $Ti_{1-y}Zr_yNiSn_{0.95}Sb_{0.05}$  series and  $L_{pure}$  is a linear fit between the mean free paths of the parent compounds  $ZrNiSn_{0.95}Sb_{0.05}$  and  $TiNiSn_{0.95}Sb_{0.05}$ , where  $1/L_{MF}$  is zero for the parent compounds ( $y=0.0$  and  $1.0$ ), indicating no mass fluctuation scattering.

In Fig. 7(b),  $1/L_{MF}$  calculated from the above equation is plotted as a function of the concentration ( $y_{Zr}$ ) of Zr substitution. Microprobe analysis in this series of compounds indicates the presence of Zr rich and Zr deficient regions. We have taken an average of the Zr concentrations ( $y_{Zr}$ ) in our calculations. The dotted curve represents  $y^*(1-y)$  function to indicate the effect of mass fluctuation scattering, where the maximum effect of mass fluctuation scattering (or minimum  $L_{MF}$ ) should be at a concentration of 50% Zr at Ti site.<sup>29</sup> The mass fluctuation scattering and  $y^*(1-y)$  behavior are also observed in our experimental measurements of the room temperature thermal conductivity values in the  $Ti_{1-y}Zr_yNiSn_{0.95}Sb_{0.05}$  series, as shown in Fig. 2(b).

## VII. CONCLUSIONS

We present two different phonon scattering mechanisms in the two different series of  $TiNiSn_{1-x}Sb_x$  and

$Ti_{1-y}Zr_yNiSn_{0.95}Sb_{0.05}$  half-Heusler alloys. In the  $TiNiSn_{1-x}Sb_x$  series, there is a direct correlation between the average grain diameter ( $D$ ) and the lattice thermal conductivity ( $\kappa_L$ ). The calculated mean free path values at  $T \approx 4$  K, where all other scattering mechanisms are a minimum, exhibit a similar correlation with the average grain sizes. Phonon boundary scattering is believed to be the prominent scattering mechanism here, when the grain size is about  $10 \mu m$  or less. In the second series of  $Ti_{1-y}Zr_yNiSn_{0.95}Sb_{0.05}$  compounds, the average grain size  $D$  is observed to be greater than  $50 \mu m$ , although the calculated mean free paths are much smaller (as low as  $L \approx 3 \mu m$  at  $T \approx 4$  K). Mass fluctuation scattering is understood to be the prominent phonon scattering mechanism in this case. There is no significant dependence of the lattice thermal conductivity on grain size in this series, indicating that phonon boundary scattering is not a prominent scattering mechanism in the Zr-substituted compounds. Our experimental results are thus in good agreement with the theoretical prediction of Goldsmid and co-workers<sup>24,25</sup> on phonon boundary scattering in the half-Heusler alloys, establishing a dependence of lattice thermal conductivity on the grain size ( $D \leq 10 \mu m$ ) in the half-Heusler alloys.

## ACKNOWLEDGMENTS

We would like to acknowledge helpful discussions with Raphael Hermann regarding mass fluctuation scattering effects in the  $Ti_{1-y}Zr_yNiSn_{0.95}Sb_{0.05}$  series. The research at Clemson University was funded in part by ONR DEPCoR program ONR (No. N00014-03-0787) and SC EPSCoR/Clemson University cost share.

\*sb7uj@virginia.edu

<sup>1</sup>J. Tabola and J. Peirre, *J. Alloys Compd.* **296**, 243 (2000).

<sup>2</sup>S. J. Poon, in *Recent Trends in Thermoelectric Materials Research I*, edited by T. M. Tritt, Semiconductors and Semimetals Vol. 70 (Academic, New York, 2001), Chap. 2, pp. 37–76.

<sup>3</sup>A. Slebarski, A. Jezierski, A. Zygmunt, S. Mähl, and M. Neumann, *Phys. Rev. B* **57**, 9544 (1998).

<sup>4</sup>S. Ögüt and K. M. Rabe, *Phys. Rev. B* **51**, 10443 (1995).

<sup>5</sup>F. G. Aliev, N. B. Brandt, V. V. Moshchalkov, V. V. Kozyrkov, R. V. Skolozdra, and A. I. Belogorokhov, *Z. Phys. B: Condens. Matter* **75**, 167 (1989).

<sup>6</sup>R. A. de Groot, F. M. Mueller, P. G. van Engen, and K. H. J. Buschow, *Phys. Rev. Lett.* **50**, 2024 (1983).

<sup>7</sup>F. G. Aliev, V. V. Kozyrkov, V. Moshchalkov, R. V. Skolozdra, and K. Durczewski, *Z. Phys. B: Condens. Matter* **80**, 353 (1990).

<sup>8</sup>C. Uher, J. Yang, S. Hu, D. T. Morelli, and G. P. Meisner, *Phys. Rev. B* **59**, 8615 (1999).

<sup>9</sup>Heinrich Hohl, Art P. Ramirez, Claudia Goldman, Gabriele Ernst, Bernd Wölfing, and Ernst Bucher, *J. Phys.: Condens. Matter* **11**, 1697 (1999).

<sup>10</sup>S. Bhattacharya, A. L. Pope, R. T. Littleton, Terry M. Tritt, V.

Ponnambalam, Y. Xia, and S. J. Poon, *Appl. Phys. Lett.* **77**, 2476 (2000).

<sup>11</sup>Q. Shen, L. Chen, T. Goto, T. Hirai, J. Yang, G. P. Meisner, and C. Uher, *Appl. Phys. Lett.* **79**, 4165 (2001).

<sup>12</sup>S. R. Culp, S. J. Poon, N. Hickman, T. M. Tritt, and J. Blumm, *Appl. Phys. Lett.* **88**, 042106 (2006).

<sup>13</sup>W. Jeitschko, *Metall. Trans.* **1**, 3159 (1970).

<sup>14</sup>S. Bhattacharya, V. Poonambalam, A. L. Pope, Y. Xia, S. J. Poon, R. T. Littleton IV, and T. M. Tritt, in *Thermoelectric Materials 2000—The Next Generation Materials for Small-Scale Refrigeration and Power Generation Applications*, edited by T. M. Tritt, G. S. Nolas, G. D. Mahan, D. Mandrus, and M. G. Kanatzidis, MRS Symposium Proceedings No. 626 (Materials Research Society, Warrendale, PA, 2000), p. Z5.2.1.

<sup>15</sup>G. D. Mahan, *J. Appl. Phys.* **65**, 1578 (1989).

<sup>16</sup>N. F. Mott, E. A. Davis, *Electronic Processes in Non-crystalline Materials* (Clarendon, Oxford 1971), p. 47.

<sup>17</sup>M. Cutler, J. F. Leavy, and R. L. Fitzpatrick, *Phys. Rev.* **133**, A1143 (1964).

<sup>18</sup>F. Gascoin, S. Ottensmann, D. Stark, S. M. Haile, and G. J. Snyder, *Adv. Funct. Mater.* **15**, 1860 (2005).

<sup>19</sup>S. Bhattacharya, Terry M. Tritt, Y. Xia, V. Ponnambalam, S. J.

- Poon, and N. Thadhani, *Appl. Phys. Lett.* **81**, 43 (2002).
- <sup>20</sup>T. M. Tritt, S. Bhattacharya, Y. Xia, V. Ponnambalam, S. J. Poon, and N. Thadhani, *Proceedings of the 27th International Thermal Conductivity Conference and the 15th International Thermal Expansion Symposium, Thermal Conductivity 27/Thermal Expansion 15*, Knoxville, TN, 2003, edited by H. Wang and W. Porter (DEStech Publications, 2004), pp. 17–31.
- <sup>21</sup>A. L. Pope, R. T. Littleton, and T. M. Tritt, *Rev. Sci. Instrum.* **72**, 3129 (2001).
- <sup>22</sup>A. L. Pope, B. Zawilski, and T. M. Tritt, *Cryogenics* **41**, 725 (2001).
- <sup>23</sup>H. J. Goldsmid, *Proc. Phys. Soc. London, Sect. B* **69**, 203 (1956).
- <sup>24</sup>J. W. Sharp, S. J. Poon, and H. J. Goldsmid, *Proceedings of the 19th International Conference of Thermoelectrics (ICT2000)*, Cardiff, Wales, 2000, edited by D. M. Rowe (Babrow, Cardiff, Wales), pp. 1–4.
- <sup>25</sup>J. W. Sharp, S. J. Poon, and H. J. Goldsmid, *Phys. Status Solidi A* **187**, 507 (2001).
- <sup>26</sup>Joseph Callaway, *Phys. Rev.* **113**, 1046 (1959).
- <sup>27</sup>S. D. Peacor, R. A. Richardson, F. Nori, and C. Uher, *Phys. Rev. B* **44**, 9508 (1991).
- <sup>28</sup>H. M. Rosenberg, in *The Solid State*, 3rd ed. (Oxford Science Publications, New York, 1988).
- <sup>29</sup>J. S. Dyck, W. Chen, C. Uher, Č. Drašar, and P. Lošt'ák, *Phys. Rev. B* **66**, 125206 (2002).
- <sup>30</sup>Standard Methods for Estimating The Average Grain Size of Metals', Approved As American Standard Z30.9–1964 by American Standards Association, ASTM Designation: E112–63, Selected ASTM Standards for Metallurgy Students, American Society for Testing and Materials, 1965, Alpha, NJ.